Viser Technology Pte. Ltd.
Research and Application of Materials Science
DOI: 10.33142/rams.v4i2.8467

Research Article Open Access

$Co_{47.5}Fe_{28.\cdot 5}Ni_{19}Si_{3.3}Al_{1.7}$ High-entropy Skeletons Fabricated by Selective Laser Melting and Properties tuned by pressure infiltration of Al

Yaqi WU[1], Yongsen CAI[1], Jinpeng HAO[1], Guihong GENG[2], Yong ZHANG[1*]

1 State Key Laboratory for Advanced Metals and Materials, University of Science and Technology Beijing, Beijing 100083, China
2 School of Materials Science and Engineering, North Minzu University, Yinchuan 750030, China

***Corresponding Author:** Yong Zhang, E-mail: drzhangy@ustb.edu.cn*

Abstract:
High saturation magnetization and low coercivity are required for soft magnetic materials. This study investigated the $Co_{47.5}Fe_{28.5}Ni_19Si_{3.3}Al_{1.7}$ high-entropy soft magnetic skeleton was prepared by selective laser melting. Then Al was pressure infiltrated into skeletons to obtain a dense composite material. The high-entropy composite materials possessed favorable compressive ductility and moderate soft magnetic properties. The high-entropy composite materials were obtained with Ms being 97.1 emu/g, 79.8 emu/g, 33 emu/g and possessing 19 Oe, 15.8Oe and 17Oe of Hc, respectively. However, the magnetostriction coefficient remains low level, about 5ppm. These reported properties are attributed to the special structure of the material studied in present experiment. Nevertheless, a novel strategy of structural designing was proposed in this paper.

***Keywords:** High entropy alloy，Composite material，Selective laser melting，gas pressure infiltration，Soft Magnetic Properties*

1 Introduction

High entropy alloys (HEAs) have attracted much attention, due to their excellent mechanical and physical properties [1-6]. The appearance of HEAs has widened the composition design space, bringing more possibilities for development of materials. Researchers have studied HEAs not only as structural materials but also as functional materials with excellent properties or the ability to serve under extreme conditions that conventional alloys cannot. With the rapid development of society, information and industrial society constantly put forward new requirements for excellent soft magnetic functional materials. Electrical and electronic equipment uses soft magnetic materials, which are easily magnetized and demagnetized [7-8]. The preparation process for silicon steel is complex and has low resistivity. Amorphous and nano soft magnetic alloys have annealed brittleness and are limited by size. Therefore, it is of great significance to develop a new kind of soft magnetic material to break through the limitations of previous materials.

Selective laser melting technology has many advantages over traditional smelting processes in terms of solidification process, thermodynamic process, microstructure, and so forth, resulting in many unique properties [9-11]. Therefore, combining it with SLM technology can produce traditional alloys and properties, such as saturation magnetic induction, coercivity, strength and plasticity, that cannot be achieved by traditional processes [12-14]. Studies about the magnetic properties of AlxCrCuFeNi2 ($0 < x < 1.5$) HEAs fabricated by laser metal deposition (LMD) [15] were founded that the FCC/L12 regions with low Al contents were weakly ferromagnetic. However, the Al-rich BCC/B2 regions were relatively soft with low coercivity, but being ferromagnetic with high saturation magnetization. When x = 1.3, the saturation magnetization and coercivity reached the maximum values, illustrating that the magnetic properties in this HEAs system could be adjusted by a paramagnetic element. In another investigation [16], the magnetic properties of AlCoxCr1-xFeNi ($0<x<1$) HEAs were researched. The results suggested that the saturation magnetization monotonically increased 6 times from 18.48 emu/g of AlCrFeNi (x=0) to 117.8 emu/g of AlCoFeNi (x=1), while the change in coercivity was non-monotonic, increasing by 7 times from AlCrFeNi (x = 0) to AlCo0.4Cr0.6FeNi (x=0.4), and then decreasing by 14 times from AlCo0.4$Cr_{0.6}$FeNi (x=0.4) to AlCoFeNi (x=1). The magnetic phase transition temperature for these HEAs showed a monotonic increasing trend with the increase of the Co content, and between x = 0.6 to x = 0.8, a secondary phase transition occurred in the composition range.

In this work, the structure of high-entropy skeleton

Received on November 14, 2022; Accepted on December 22, 2022

was designed and prepared by selective laser melting (SLM), and high-entropy composite materials were prepared by pressure infiltration process, so as to improve the mechanical properties of the skeleton structure.

2 Materials and methods

2.1 Alloys Preparation

316L stainless steel (100*100*20mm^3) was used for the substrate in the SLM technology forming process. Gas atomization and high-purity $Co_{47.5}Fe_{28.5}Ni_{19}Si_{3.3}Al_{1.7}$ HEA powders was used for SLM and its composition has been listed in Table 1. The powder particle size range is about 15-53 um which microstructure was shown in figure 1. Here, three types skeleton structures were designed for the following work of gas pressure infiltration. The skeleton models firstly were created by the SolidWorks software. As shown in the figure 2, the total size of the model is a square with 10*10*10mm3 size, but possessing different square-pore size and they are 0.6 mm, 0.7 mm, 0.8 mm, respectively. All skeleton samples were prepared by AFS-M120 SLM equipment produced by Longyuan AFS Co., Ltd.

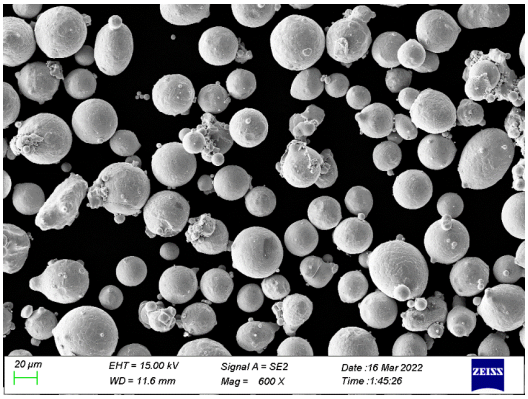

Figure 1 Microstructure of $Co_{47.5}Fe_{28.5}Ni_{19}Si_{3.3}Al_{1.7}$ powders

Table 1 Compositions of the $Co_{47.5}Fe_{28.5}Ni_{19}Si_{3.3}Al_{1.7}$ HEA powders

Elements	Co	Fe	Ni	Si	Al
Atomic ratio (at. %)	47.5	28.5	19.0	3.3	1.7

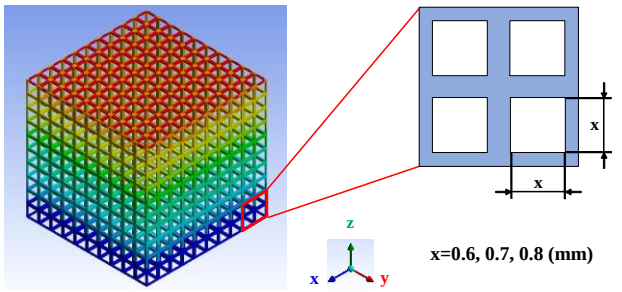

Figure 2 Schematic diagram of the porous structure of three types of high-entropy seleton with different square-pore sizes

Subsequently, pressure infiltration was carried out under high purity Ar atmosphere. Put the pure Al and $Co_{47.5}Fe_{28.5}Ni_{19}Si_{3.3}Al_{1.7}$ HEA skeleton into the pressure infiltration equipment, heating up the equipment to 800 degrees Celsius and keeping warm for 0.5 hours. After the Al melted, applied a pressure of 1 MPa to pressed Al into the high-entropy skeletons, followed by stopping heating and pressurizing when it was completed, then cooled down with the furnace.

2.2 Structural Characterization and Performance Experiments

A Bruker D8 Smart Lab X-ray diffractometer was utilized to determine the crystal structure, with Cu-Kα radiation ranging from 20° - 90°. The scanning rapid is 10°/min. The microstructure characterization and electron backscatter diffraction were measured using scanning-electron microscopy (SEM) with Zeiss Supera55 operated at 20 keV, along with energy-dispersive spectrometry (EDS). Compressive simples were a cylinder with φ3 × 6 mm cut by electro-discharge machining and compressive tests at strain rate of 5×10-3s-1 and 5×10-4s-1 for high-entropy skeleton and high-entropy composites, using CMT Model 4305 Universal Electronic Tester at room temperature respectively. The soft magnetic properties of samples with 3mm×2mm×2mm sizes were measured by vibrating sample magnetometer (VSM) under a magnetic field of ±1T at room temperature. The magnetostriction coefficient was obtained by the resistance strain gauge method.

3 Results and discussion

3.1 Phase formation and microstructure

We investigated the microstructure, compressive properties and soft magnetic properties of Al-$Co_{47.5}Fe_{28.5}Ni_{19}Si_{3.3}Al_{1.7}$ high-entropy composites structural material. Figure 3 is the macrostructure of the $Co_{47.5}Fe_{28.5}Ni_{19}Si_{3.3}Al_{1.7}$ high-entropy skeleton prepar ed by SLM.

The XRD pattern of high-entropy skeleton and high-entropy composites materials were shown in the figure 4(a) and figure 4(b). It is clearly shown that the main phase, a single face centered cubic (FCC) crystal of the skeleton, was identified. While several small peaks of compound phases appeared after pressure infiltration of aluminum. The X-ray diffraction analysis indicates that the porous material with high entropy only has one FCC phase, because the three phases of Fe, Co, and Ni dissolve into one solid solution, and trace amounts of Al and Si do not affect the overall FCC solid solution structure, and a single FCC solid solution performs.

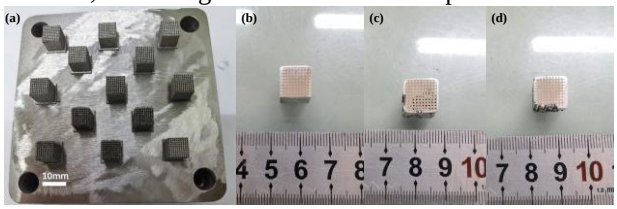

Figure 3 Macrostructure images of high-entropy skeletons prepared by SLM. (a) is high-entropy skeletons;(b)-(d)are high-entropy composite materials

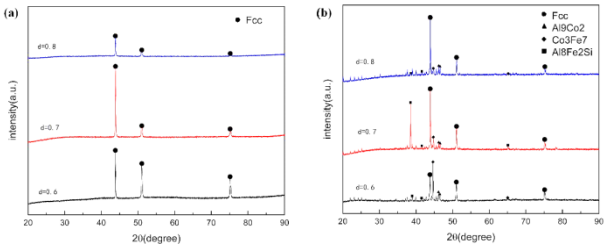

Figure 4 (a)X-ray diffraction patterns of $Co_{47.5}Fe_{28.5}Ni_{19}Si_{3.3}Al_{1.7}$ HEAs pores prepared by SLM with different side lengths and sizes of skeleton structures. (b)X-ray diffraction patterns of $Co_{47.5}Fe_{28.5}Ni_{19}Si_{3.3}Al_{1.7}$ high-entropy composites prepared by air pressure infiltration process

SEM images of high-entropy skeletons are presented in figure 5(1-a)-5(1-f), which exhibit smooth surface morphologies with the square shape of 0.6mm, 0.7mm and 0.8mm respectively. The cleary molten pool on the cross-section presents a classic scaly which are observed from figure 5(1-b), (1-d), (1-f). EBSD mapping as displaying in the figure 5(2), demonstrates that the high-entropy skeleton structure is a polycrystalline structure with the grain size between tens and two hundred microns. In areas A and B away from the boundary of the square-pores, the grains are relatively large. Moreover, in the central region A of the high-entropy skeleton, the grain size is relatively large, around 200 um. And the grain size is about 50 um in the suspension region B It can be seen that with the increasing of the square-pore size, the grain size tends to be uniform gradually. Figure 6 (2). EDS mapping illustrated that the five elements of Fe, Co, Ni, Al and Si are evenly distributed without element segregation in the high-entropy composite materials. The same as the results of the above SEM and XRD analysis.

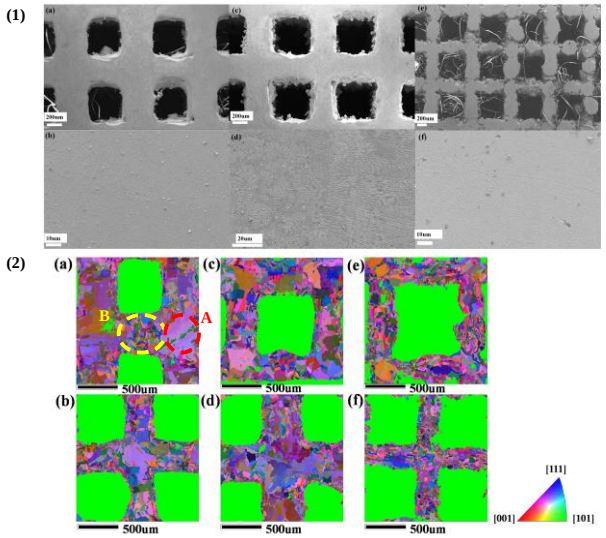

Figure 5 (1):SEM image of $Co_{47.5}Fe_{28.5}Ni_{19}Si_{3.3}Al_{1.7}$ high-entropy skeleton with different square-pore sizes(a)(b) the side length of the square-pore is 0.6 mm; (c)(d) the side length of the square-pore is 0.7 mm; (e)(f) the side length of the square-pore is 0.8 mm. (2): EBSD mapping of high-entropy skeleton

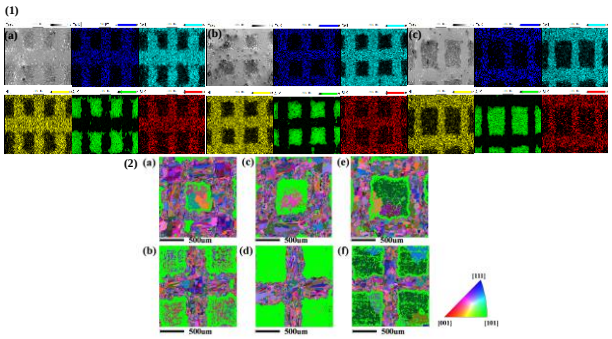

Figure 6 EDS and EBSD mapping of high-entropy composite with differen square size. (1-a)-(1-c) show the elemnts distrbution of high-entropy composites with different square-pores. (2) is the EBSD results of high-entropy composites materials

Owing to the high cooling rate (105 ～ 106 K/s) of the SLM process, the SLM Co47.5Fe28.5Ni19Si3.3Al1.7 alloy skeleton formed a non-equilibrium solidification organization, and this inhomogeneous tissue distribution can be attributed to the variation of local solidification conditions, which includes the temperature gradient (G) and solidification rate (R). The G/R value is determined by the undercooling of the composition at the solidification front of the melt pool, which in turn determines the morphology of the solidification structure. At the boundary of the molten pool, the heat of the melt can be conducted and dissipated through the SLM forming substrate. In the case of a single melt pool, the heat of the melt pool is first transferred to the solidified portion of the melt pool boundary [17-18].

The formation of large columnar grains in the middle of the melt pool, the heat-affected zone near the melt pool boundary is distributed with very fine equiaxed grains, and welding fusion zone structure is similar [19].

3.2 Mechanical properties

Compressive strain curves measured at room temperature (298K) are plotted in the figure 7. With the increasing of square-pores size, the strength of HEA-skeletons decreases. The slope decreases following the square-pore size increasing, which illustrates that as the square-pore size grows lager the Yong's modulus decreases. The same trends were observed from compressive strain curves of $Co_{47.5}Fe_{28.5}Ni_{19}Si_{3.3}Al_{1.7}$ high-entropy composite materials. Mechanical properties dates of high-entropy skeleton and composite materials were shown in Table 1. It can be observed that the strength increased and existed typical yield phenomenon obviously after infiltration of aluminum. In addition, HEA composites material performed excellent compressive ductility with loading increasing.

During the compression process, pores of different sizes reduce the load-bearing area, and also increase the loading stress initiating and promoting crack propagation, leading to premature failure of SLM-fabricated [20] With the pores being filled by Al, improved strength of the composite materials. On the other hand, the aluminum

element diffuses into the high-entropy alloy skeleton during the pressure infiltration process, forming intermetallic compounds of aluminum, which makes the dislocation movement hindered by grain boundaries and therefore increases the strength.

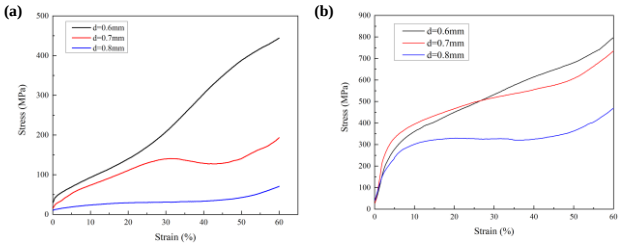

Figure 7 Compressive stress-strain curves of $Co_{47.5}Fe_{28.5}Ni_{19}Si_{3.3}Al_{1.7}$ HEAs skeleton and composites after infiltration at room temperature. (a): Properties of $Co_{47.5}Fe_{28.5}Ni_{19}Si_{3.3}Al_{1.7}$ HEAs skeleton. (b): Properties of $Co_{47.5}Fe_{28.5}Ni_{19}Si_{3.3}Al_{1.7}$ HEAs composites

3.3 Magnetic properties

The saturation magnetization and coercivity curves of HEA skeleton and composites can be obtained from figure 8(a) and (b). Figure 8(c) and (d) dispaly the Hc and Ms values bar of of high-entropy skeleton and composites respectively. According to figure 8, the saturation magnetizations of high-entropy skeletons fabricated by selective laser melting, are 146.2emu/g, 146.8emu/g and 151.3emu/g respectively. Experimental results were closed to that prepared by magnetic levitation melting we investigated in previous work [8].And the coercivity reaches14Oe, 9.9Oe, and 7.2Oe, respectively. After pressure infiltration of Al, values of Ms decreased markedly and Hc increased slightly. The Ms of the High-entropy composite materials are 97.1 emu/g, 79.8 emu/g, 33 emu/g and possess 19 Oe, 15.8Oe and 17Oe of Hc, respectively. The coercivity of the three composite materials is obviously larger than the limit value of soft magnetic materials (＜1000 A/m or 12.56 Oe).

Table 2 Compressive properties of $Co_{47.5}Fe_{28.5}Ni_{19}Si_{3.3}Al_{1.7}$ HEAs skeleton and composites after infiltration at room temperature.

d(mm)	$\sigma_{0.2}$(MPa)/ε_p(%) (HEA-skeleton)	$\sigma_{0.2}$(MPa)/ε_p(%) (HEA composites material)
0.6	45.6＞60%	240/＞60%
0.7	28.5＞60%	277.9/＞60%
0.8	13 ＞60%	198/＞60%

The saturation magnetization strength of soft magnetic materials is related to the constituent elements of the alloy [7, 21]. In the present experiment, the saturation magnetization strength of the high-entropy skeleton is comparable to that of the as-cast alloy, while the saturation magnetization strength decreases after pressure infiltration due to the fact that Al is a paramagnetic element with a magnetic moment close to 0, which leads to a decrease in saturation magnetization strength as the Al content increases [22]. The difference is that grain size and defects have a greater effect on the coercivity of the alloy.

It is known that the magnetic property of materials is dependent on the magnetic domains, in which the internal stress induced by crystalline defects could block the movement of domain walls in an applied magnetic field, leading to in an increase in the coercivity Hc. The grain size of the alloy prepared by SLM is around 100um [8], which is comparable to the cast state and therefore the coercivity is closer. It indicates that defects become the main influencing factor for the similar grain size. In this work, square-pores structure with different sizes in the high-entropy skeleton can be regarded as a macroscopic defect that causes a major shielding effect on the motion of magnetic domains.

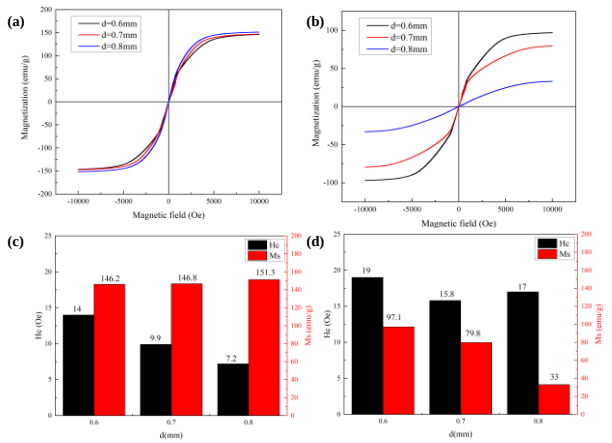

Figure 8 Room temperature hysteresis loops of $Co_{47.5}Fe_{28.5}Ni_{19}Si_{3.3}Al_{1.7}$ HEAs skeleton and composites

3.4 Magnetostriction characterization

Magnetostrictive coefficient curve are given in Figure 9 for $Co_{47.5}Fe_{28.5}Ni_{19}Si_{3.3}Al_{1.7}$ high-entropy skeleton and composite materials. It was found that the magnetostrictive coefficients of high-entropy skeleton and composite materials remained at the stable level, about 10 ppm and 5 ppm respectively. In comparison, the alloys $Co_{47.5}Fe_{28.5}Ni_{19}Si_{3.3}Al_{1.7}$ prepared by SLM in the present study possessed lower magnetostrictive performance than smelted by magnetic levitation [8].

Magnetostriction is the mechanical vibration of a material at the same frequency as the magnetic field under the action of an alternating magnetic field, i.e., the conversion of electromagnetic energy into mechanical energy. The magnetostriction coefficient is large, and the vibration generated by the conversion of mechanical energy is larger when the device is in operation, there will be noise generated. Hence, a lower magnetostriction coefficient will reduce the mechanical energy conversion and reduce the noise.

A number of researches indicated that prepared by SLM in the present study possessed better magnetostrictive performance than as-cast. For instance, Zhang et al. prepared bulk Fe-Ga alloys with 12 mm in diameter and 2 mm in thickness by casting and aging for 24 h. It was found that the λ//s (positive saturated magnetostriction) for the alloy with a thickness of 2 mm was 32 ppm and gradually increased with the thinning of

the alloy [23]. In addition, oriented bulk Fe-Ga rods prepared by directional solidification method, which showed large columnar crystals with ＜ 100 ＞ preferential orientation and a magnetostriction of 170 ppm [24]. However, in contrast to reported, the magnetostriction coefficients in present study were reduced. On the one hand, SLM process reduces the magnetostriction of the $Co_{47.5}Fe_{28.5}Ni_{19}Si_{3.3}Al_{1.7}$ skeleton and increases the blockage of the magnetic domain wall by irregular grains, which is not conducive to the uniform motion of the magnetic domain wall [25]. On the other hand, the special structure of the high-entropy skeleton impedes the movement of the magnetic domain walls, thus weakening the magnetostriction phenomenon of the alloy [26].

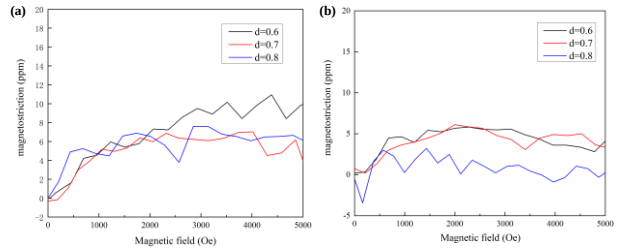

Figure 9 Magnetostrictive curves of $Co_{47.5}Fe_{28.5}Ni_{19}Si_{3.3}Al_{1.7}$ high-entropy skeletons and high-entropy composites materials.

4 Conclusions

This paper presents research on $Co_{47.5}Fe_{28.5}Ni_{19}Si_{3.3}Al_{1.7}$ high-entropy composites were prepared by selective laser melting and pressure infiltration. we developed three different high-entropy square-pore structures and composite materials. The following conclusions were drawn:

(1) $Co_{47.5}Fe_{28.5}Ni_{19}Si_{3.3}Al_{1.7}$ high-entropy skeleton were prepared by selective laser melting with a single FCC phase. And the compound phase of Al appears in the composite after Al pressure infiltration.

(2) Uneven grain size of the high entropy skeleton structure is the result of non-equilibrium solidification caused by the different cooling rates between the center and the boundary of the melt pool in the SLM process.

(3) The saturation magnetization strength decreases after pressure infiltration due to the fact that Al is a paramagnetic element with a magnetic moment close to 0, which leads to a decrease in saturation magnetization strength as the Al content increases. For the similar grain size, defects become the main influencing factor. In this work, square-pores structure with different sizes in the high-entropy skeleton can be regarded as a macroscopic defect that causes a major shielding effect on the motion of magnetic domains.

(4) The composites with different square-pore sizes exhibit favorable compressive plasticity with a degree of deformation above 60%. Strength of high-entropy composite materials was improved due to infiltration of Al into pore defects.

(5) The magnetostriction coefficient of high-entropy composite material is lower than that of high-entropy skeletons, but the magnetostriction coefficients of both are relatively low and more stable.

DECLARATIONS

Authors' contributions

Made substantial contributions to conception and design of the study and performed data analysis and interpretation: Yaqi Wu, Yongsen Cai, Jinpeng Hao; rovided technical, and material support: Yong Zhang.

Availability of data and materials

Not applicable.

Financial support and sponsorship

Y. Z. acknowledges supports from (1) National Natural Science Foundation of China (NSFC, Granted Nos. 51671020); (2) Guangdong Basic and Applied Basic Research Foundation (No.2019B1515120020); and (3) Creative Research Groups of China (No.51921001).

Conflicts of interest

All authors declared that there are no conflicts of interest.

References

[1] Zhang Y, Amorphous and High entropy alloys. China Science Publishing & Media Ltd; 2010(1):125-130.

[2] Beke D L, Erdélyi G. On the diffusion in High entropy alloys [J]. Materials Letters 2016(164): 111-113.

[3] Gao M C, Liaw P K, Yeh J W, et al.. High entropy alloys: Fundamentals and applications [J]. 2016(1), 210-221.

[4] Gao M C, Miracle D B, Maurice D, et al.. High-entropy functional materials. Journal of Materials Research 2018, 33(19): 3138-3155.

[5] Xue H Y, Jin S L, Wei R Z, et al.. A Brief Review of High-Entropy Films [J]. Journal of Materials Chemistry and Physics, 2017(1): 210.

[6] Yeh J W, Chen S K, Lin S J, et al.. Nanostructured High entropy alloys with Multiple Principal Elements: Novel Alloy Design Concepts and Outcomes. Advanced Engineering Materials 2004, 6(5): 299-303.

[7] Herzer G. Modern soft magnets: Amorphous and nanocrystalline materials. Acta Materialia 2013, 61(3): 718-734.

[8] Zhang Y, Zhang M, Li D Y, et al.. Metals Compositional Design of Soft Magnetic High Entropy Alloys by Minimizing Magnetostriction Coefficient in (Fe0.3Co0.5Ni0.2)100 − x(Al1/3Si2/3)x System [J]. 2019, 9(3):5-6.

[9] D. Herzog, V. Seyda, E. Wycisk, et al.. Additive manufacturing of metals [J]. Acta Mater, 2016(117): 371-392.

[10] S. Chen, Y. Tong, P. Liaw, Additive manufacturing of high-entropy alloys: A review [J]. Entropy, 2018, 20(12): 937.

[11] H. Dobbelstein, E.L. Gurevich, E.P. George, et al.. Laser metal deposition of compositionally graded TiZrNbTa

refractory high-entropy alloys using elemental powder blends [J]. Addit. Manuf, 2019(25):252-262.

[12] L C Huang, Y N Sun, A. Abdukadir, et al.. Microstructure and mechanical properties of AlxCoCrFeNi High entropy alloys deposited by laser melting [J]. Vaccum, 2021(183):109875.

[13] Wang S, Liu Y D, Qi B, et al.. Study on the forming process and performance of 316L large layer thickness by selective laser melting [J]. Applied Laser, 2017, 37(6):7.

[14] Wang Z K, Zheng Q G, Wang T, et al.. Coagulation tissue feature formation process of laser surface cladding layer [J]. Laser technology 2000(1):66-68.

[15] T. Borkar, B. Gwalani, D. Choudhuri, et al.. A combinatorial assessment of AlxCrCuFeNi2 (0 ＜ x ＜ 1.5) complex concentrated alloys: microstructure, microhardness, and magnetic properties [J]. Acta Mater,2016(6):63-76.

[16] T. Borkar, V. Chaudhary, B. Gwalani, et al.. A combinatorial approach for assessing the magnetic properties of high entropy alloys: role of Cr in AlCoxCr1-xFeNi (0＜x＜1.5) [J]. Adv. Eng. Mater, 2017, 19 (8):1700048.

[17] Carter L N, Withers P J, Martin C. The influence of the laser scan strategy on grain structure and cracking behaviour in SLM powder-bed fabricated nickel superalloy [J]. Journal of Alloys and Compounds, 2014(615):338-347.

[18] Y.Y. Chen, H. Yue, X.P. Wang. Microstructure, texture and tensile property as a function of scanning speed of Ti47Al2Cr2Nb alloy fabricated by selective electron beam melting [J]. Mater. Sci. Eng. A, 2018(713):195-205.

[19] S.J. Wolff, S. Lin, E.J. Faierson, et al.. A framework to link localized cooling and properties of directed energy deposition (DED)-processed Ti-6Al-4V [J]. Acta Mater. 2017(132): 106-17.

[20] L. Lan, W. Wang, Z. Cui, et al.. Anisotropy study of the microstructure and properties of AlCoCrFeNi2.1 eutectic high entropy alloy additively manufactured by selective laser melting[J]. J. Mater. Sci. Technol., 2022(129):229-239.

[21] Huang B, Yang Y, Wang A D, et al.. Saturated magnetization and glass forming ability of soft magnetic Fe-based metallic glasses [J]. Intermetallics 2017(84):74-81.

[22] Zhang Y, Zuo T T, Cheng Y Q, et al.. High entropy alloys with High Saturation Magnetization[J]. Electrical Resistivity, and Malleability. Scientific Reports 2013(3):1455.

[23] J.H. Li, X.X. Gao, X.M. Xiao, et al.. M.-C. Zhang, Magnetostriction of ＜100＞ oriented Fe-Ga rods with large diameter [J]. Rare Met, 2015, 34 (7):472-476.

[24] Y. Zhang, P. Sun, J. Gou, et al.. Depth-dependent decomposition and property of large magneto-striction Fe-Ga alloys [J]. Appl. Surf. Sci, 2021(569):151059.

[25] G.D. Liu, X.F. Dai, Z.H. Liu, et al.. Structure, magnetostriction, and magnetic properties of melt-spun Fe-Ga alloys [J]. J. Appl. Phys, 2016, 99 (9):093904.

[26] A.A. Emdadi, S.H. Nedjad, H.B. Ghavifekr. Effect of solidification texture on the magnetostrictive behavior of galfenol [J]. Metall. Mater. Trans. A, 2014, 45 (2): 906-910